***JKPK (JURNAL KIMIA DAN PENDIDIKAN KIMIA)**, Vol. 11, No. 2, 2026* *pp. 267-286*
Chemistry Education Study Program, Universitas Sebelas Maret *ISSN 2503-4146*
https://jurnal.uns.ac.id/jkpk *ISSN 2503-4154 (online)*

Green-Synthesized Silver Nanoparticles from *Ocimum sanctum* Leaf Extract for a Chitosan–Starch Colorimetric Hg^{2+} Sensor

Yussi Pratiwi[1], Fuad Alfan Asyifa[1], Agus Darmawan[1], Harfi Amania Khansa[1]*, Elsa Vera Nanda[1], Baiq Amelia Riyandari[2], Aneesha Sheik Musthafa Ajeetha[3]

[1]Department of Chemistry, Faculty Mathematics and Sciences, Universitas Negeri Jakarta, Jakarta, Indonesia.
[2]Department of Chemistry Education, Faculty of Education and Teacher Training, Universitas Islam Negeri Mataram, Indonesia.
[3]Department of Chemistry, Karpagam Academy of Higher Education, Coimbature, India

ABSTRACT

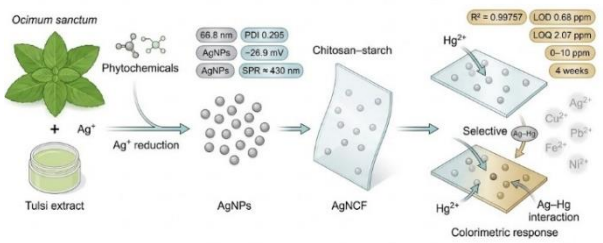

The presence of Hg^{2+} ions in soil and water poses a potential risk to living organisms, including humans, necessitating simple and accessible detection methods. This study evaluated *Ocimum sanctum* (Tulsi) leaf extract as a reducing and stabilizing agent for the green synthesis of silver nanoparticles (AgNPs) and subsequently developed a chitosan-starch nanocomposite film for the colorimetric detection of Hg^{2+}. AgNPs produced using various extract preparation methods were comparatively evaluated based on their physicochemical characteristics and colloidal stability. AgNPs with the most suitable properties were selected for incorporation into the nanocomposite film. The selected AgNPs exhibited a particle size of 66.8 nm, a polydispersity index of 0.295, and a zeta potential of −26.9 mV, indicating a relatively uniform particle distribution and moderate colloidal stability. The AgNPs-loaded chitosan-starch nanocomposite film demonstrated a selective colorimetric response to Hg^{2+} under the tested conditions, with a linear response across the Hg^{2+} concentration range of 0–10 ppm. The sensor exhibited a limit of detection of 0.68 ppm and a limit of quantification of 2.07 ppm, while maintaining its detection performance for up to four weeks. These findings highlight the potential of plant-synthesized AgNPs incorporated into a chitosan-starch matrix as a simple colorimetric platform for Hg^{2+} detection.

Keywords: *colorimetric sensor; Hg^{2+} detection; silver nanoparticles; tulsi leaf extract*
**Corresponding Author:* *harfi.amania@gmail.com*
How to cite: Y. Pratiwi, F. A. Asyifa, A. Darmawan, H. A. Khansa, E. V. Nanda, B. A. Riyandari, and A. S. M. Ajeetha, "Green-Synthesized Silver Nanoparticles from Ocimum sanctum Leaf Extract for a Chitosan–Starch Colorimetric Hg^{2+} Sensor," *Jurnal Kimia dan Pendidikan Kimia (JKPK)*, vol. 11, no. 2, pp. 267–286, 2026. [Online]. Available: https://doi.org/10.20961/jkpk.v11i2.119903
Received: 2026-05-26 *Accepted: 2026-08-11* *Published: 2026-08-31*

INTRODUCTION

Intensive industrial, agricultural, and urbanisation activities contribute to environmental pollution, particularly the contamination of aquatic environments by highly toxic heavy metals. Some heavy metals, such as lead (Pb) and arsenic (As), are toxic even at very low concentrations [1]. Mercury (Hg) is a highly toxic heavy metal because of its neurotoxic effects on living organisms, including humans. Moreover, mercury is difficult to degrade once it enters aquatic environments. It is not only present in the water column but can also accumulate in sediments [2]. Government Regulation Number 22 of 2021 concerning the Implementation of Environmental Protection and Management stipulates a maximum mercury concentration in water of 0.002 ppm [3]. The Cilemahabang River in Bekasi,

Indonesia, has been reported to contain mercury at a concentration of approximately 0.0031 ppm [4]. This concentration exceeds the regulatory limit established by the government.

Mercury can be detected using various analytical instruments, such as Inductively Coupled Plasma Mass Spectrometry (ICP-MS) and Atomic Absorption Spectrophotometry (AAS). However, determining heavy metal concentrations in environmental samples using these techniques requires specialized expertise and can be time-consuming. These limitations may restrict their widespread application when rapid and convenient detection is required. Therefore, alternative methods for mercury analysis that are more efficient and effective for both qualitative and quantitative detection are needed, including approaches based on silver nanoparticles (AgNPs) [5]. AgNP-based colorimetric sensors offer several advantages, including rapid visual detection and relatively low cost [6]. AgNPs have been widely investigated for heavy metal detection. Previous research has successfully synthesized AgNP-based colorimetric sensors for detecting mercury ions (Hg2+) using lemongrass leaf extract as a reducing agent, while another study used Kokum fruit extract to synthesize anionic AgNPs for mercury ion (Hg2+) detection [7], [8]. AgNP-based colorimetric sensors exhibit excellent performance in detecting metal ions because of their localized surface plasmon resonance (LSPR) properties, which enable visually observable color changes in response to environmental changes, such as the introduction of an analyte [9].

The synthesis of AgNPs can be carried out using various physicochemical methods. Plant extract-mediated synthesis has emerged as an alternative approach for synthesizing silver nanoparticles (AgNPs) because phytochemicals, such as flavonoids, phenolics, and other secondary metabolites, can act as reducing and stabilizing agents, thereby reducing reliance on additional synthetic reducing chemicals [10], [11]. However, this approach should not automatically be considered sustainable or environmentally friendly, as the overall process may still involve the use of organic solvents during extract preparation, silver precursors derived from AgNO3, energy-intensive heating or solvent evaporation, and the generation of silver-containing waste that requires proper treatment [11]. Therefore, although plant extracts offer a promising alternative for nanoparticle synthesis, the sustainability of the overall process should be comprehensively evaluated by considering raw materials, solvent selection, energy consumption, waste management, and the environmental risks associated with silver nanoparticles.

Numerous plant extracts have been utilized for the synthesis of AgNPs, including *Ocimum sanctum* (Tulsi) extract, which has been used to produce AgNPs with particle sizes ranging from 15 to 35 nm [12]. Tulsi leaves contain phytochemical compounds such as polyphenols and flavonoids that possess numerous hydroxyl groups and can function as effective reducing agents [13], [14]. Although plant extracts have been widely used in AgNP synthesis, comparative studies of AgNPs synthesized using unfractionated and

fractionated extracts remain limited. Most previous studies have used crude extracts without applying a fractionation process to remove substances that may not be required for AgNP synthesis [15]. The resulting AgNPs can subsequently be incorporated into nanocomposite films to improve their stability for sensor applications. One approach involves incorporating AgNPs into a chitosan-starch matrix, which has not been widely investigated [16].

This study aimed to synthesize AgNPs using unfractionated and fractionated Tulsi leaf extracts as reducing agents, with glucose as a stabilizing agent. Tulsi leaf extracts were analyzed using thin-layer chromatography (TLC) and Liquid Chromatography-Mass Spectrometry (LC-MS) to identify the phytochemical compounds present in the extracts. The resulting AgNPs were characterized using several analytical techniques, including UV-Vis spectrophotometry, Particle Size Analysis (PSA), and Fourier Transform Infrared (FTIR) spectroscopy. AgNPs with the most suitable properties were subsequently incorporated into a chitosan-starch nanocomposite film. The resulting film was characterized using X-Ray Diffraction (XRD) and Scanning Electron Microscopy-Energy Dispersive X-Ray (SEM-EDX) analysis, and its performance as a selective colorimetric sensor for Hg2+ was evaluated in terms of selectivity, interference, response time, linearity, sensitivity, Limit of Detection (LOD), and Limit of Quantification (LOQ).

METHODS

1. Materials and Instruments

The materials used in this study included Tulsi leaves (Ocimum sanctum) obtained from the Bekasi area, ethyl acetate (≥99.5% purity Merck, Germany),, methanol (≥99.9% purity Merck, Germany), n-hexane (≥99.0% purity Merck, Germany), AgNO3 (≥99.8% purity Merck, Germany), dextrose (α-D-glucose) (≥97.5% purity Merck, Germany), starch (≥98.0% purity Merck, Germany), chitosan (≥75% purity Sigma Aldrich, USA), acetic acid glacial (≥99% purity Merck, Germany), ethanolic AlCl3 (1% w/v solution), and analytical-grade metal salts including HgCl2, AlCl3, CuSO4.5H2O, MnSO4.2H2O, Pb(NO3)2, 3CdSO4.8H2O, NaNO3, FeSO4.7H2O, MgSO4.7H2O, NiSO4.6H2O, Co(NO3)2.6H2O, BaCl2.2H2O (≥99% purity Merck, Germany).

The instruments used in this study were UV-Vis spectrophotometer (Shimadzu UV-1900i), Liquid Chromatography-Mass Spectrometry (LC-MS) (Acquity UPLC H-Class System), Particle Size Analyzer (PSA) (Horiba Scientific SZ 100z), Fourier Transform Infrared (FTIR) spectrophotometer (Shimadzu IR Spirit), Scanning Electron Microscope-Energy Dispersive X-ray Spectroscopy (SEM-EDX) (Quattro S. Thermo Scientific), and X-ray Diffraction (XRD) (Thermo Fisher Scientific).

2. Preparation of Tulsi Leaf Extract

Tulsi leaves were washed several times with an aquadest to remove impurities, then dried in an oven at 60^{o}C and ground until it becomes a powder. Then 8 g of powdered leaves were added to 160 mL of water and heated at 60^{o}C for 10 minutes. The mixed

solution that has been completed was then filtered using Whatman filter paper No. 42 to obtain a solution of Tulsi leaf extract. Subsequently, this filtrate (the unfractionated stock extract solution) was diluted to 8% v/v and stored at 25°C. The remaining aqueous extract was subjected to fractionation via liquid-liquid extraction.

3. Extract Fractionation by Liquid-Liquid Extraction

The aqueous extract underwent liquid-liquid fractionation using ethyl acetate to enrich the phytochemical content based on polarity. Briefly, 100 mL of the aqueous extract was placed in a separatory funnel and extracted with 200 mL of ethyl acetate (1:2, v/v). The ethyl acetate layer was collected, while the remaining aqueous phase was re-extracted three times using fresh ethyl acetate under the same conditions. The pooled ethyl acetate fractions were concentrated using a rotary evaporator until the solvent had completely evaporated, yielding 71 mg of the dry ethyl acetate fraction. This dry fraction was then redissolved in 71 mL of methanol to prepare 1000 ppm stock of the fractionated extract for AgNPs synthesis. The resulting fractionated extract was stored in an amber bottle at 4°C for 3 days prior to use. The concentration of the fractionated extract used for AgNPs synthesis was 80 ppm.

4. Flavonoid Test of Tulsi Leaf Extract by TLC

Silica gel plates (2.5×8 cm) were prepared with upper and lower margins of 1 cm. The mobile phase consisted of n-hexane and ethyl acetate (1:1, v/v) was used. The sample was spotted onto the silica plate and placed in the TLC chamber. After the solvent reached the upper mark, the plate was removed from the chamber and air-dried at room temperature. A 1% $AlCl_3$ solution in ethanol was used as a detecting reagent for flavonoids. The appearance of yellow spots indicated the presence of flavonoids[17]. The yellow spots were marked, and their migration distances were measured to determine the retention factor (Rf) values. UV light at a wavelength of 254 nm was also used to observe the separation results.

5. Characterization of Tulsi Leaf Extract Using LC-MS

Chromatographic separation was performed using an ACQUITY UPLC® H-Class system (Waters, Milford, MA, USA) equipped with an ACQUITY UPLC® BEH C18 column (2.1 × 100 mm, 1.7 µm) maintained at 50°C. The mobile phase consisted of water containing 5 mM ammonium formate (A) and acetonitrile containing 0.05% formic acid (B), delivered at a flow rate of 0.2 mL min^{-1} using a 23-minute gradient elution program. Samples were filtered using a 0.2 µm syringe filter, and a 5 µL aliquot was injected into the system. Mass spectrometric detection was performed using a Waters Xevo G2-S QTof mass spectrometer equipped with an electrospray ionization (ESI) source operating in positive ion mode over an m/z range of 50–1300. The source temperature was maintained at 100°C, desolvation temperature at 350°C, cone gas flow rate at 0 L h^{-1}, and desolvation gas flow rate at 793 L h^{-1}. Data acquisition was performed using MassLynx software, applying low and high

collision energy functions of 4 V and 25–70 V, respectively.

6. Synthesis of AgNPs

AgNPs synthesis was carried out by adjusting the precursor concentration, pH, temperature, and stirring time. For AgNPs synthesized using unfractionated extract, 3 mM $AgNO_3$ was reacted with the unfractionated extract at a concentration of 8% (v/v). Meanwhile, for AgNPs synthesized using fractionated extract, 10 mM $AgNO_3$ was reacted with the fractionated extract at a concentration of 80 ppm. All experiments were conducted in a 10 mL solution with the addition of 0.18% glucose at pH 8 and a temperature of 55^oC for 75-120 minutes reaction time.

7. Characterization of AgNPs

SPR spectra in the wavelength range of 300–600 nm was used to determine the SPR band using a Shimadzu UV-1900I spectrophotometer. Functional groups were identified using a Shimadzu IR Spirit spectrometer within the range of 5000–400 cm^{-1}. A Horiba SZ-100 instrument was used to determine the particle size and zeta potential of the nanoparticles at a scattering angle of 90^o with a holder temperature of 25^oC and three test repetitions. Data analysis and graphical interpretation were performed using OriginPro 2018 software.

8. Preparation of Nanocomposite Film

A chitosan stock solution was prepared by dissolving 3 g of chitosan powder (molecular weight: ~198 gram/mol, degree of acetylation: ~87.5%) was dissolved in 150 mL of 1% acetic acid and stirred until homogeneous. Similarly, to prepare a starch stock solution, 1.5 g of starch soluble (pro analysis) was dissolved in 80 mL of distilled water, maintaining the temperature at 60-80°C and stirring continuously until the cloudy white solution became transparent (approximately 1 hour), and then cooled to room temperature. To prepare a chitosan-starch-Ag nanocomposite film (AgNCF), 20 mL of chitosan and 20 mL of starch were mixed and stirred to obtain a homogeneous sample (1:1 dry polimer ratio). 7 mL of AgNPs solution (prepared using 10 mM $AgNO_3$ and 8% v/v unfractionated extract) was added and stirred for 10 minutes. The film was poured into a petri dish (Ø100 mm x 18 mm, corresponding to a casting area of 78.5 cm^2) and heated at 60^oC in an oven for 24 hours. The film was then removed from the petri dish at room temperature and stored in a desiccator for later use.

9. Characterization of AgNCF

SPR spectra in the wavelength range of 300–600 nm was used to determine the SPR band using a Shimadzu UV-1900I spectrophotometer. Functional groups were identified using a Shimadzu IR Spirit spectrometer within the range of 5000–400 cm^{-1}. The characteristics of the crystal structure of the film were analyzed using a Thermo Fisher Scientific XRD. Quattro S. Thermo Scientific SEM-EDX was used to analyze the surface characteristics and elemental composition analysis on the film surface. Data analysis and graphical interpretation were performed using OriginPro 2018 software.

10. Sensor Performance Tests

The method validation test includes selectivity, interference, sensitivity, and linearity test, as well as LOD and LOQ. Stability tests were carried out by measuring the SPR band of nanocomposite film up to week 4, while sensor response time tests were carried out by measuring the time required for the film to produce a stable color after being dipped in 3 mL selected metal ions. As for selectivity test, metal ions were mixed with nanoparticles at a ratio of 2:1 (v/v), while the nanocomposite film was dipped into 3 mL of metal ion solutions. All metal ion solutions were prepared in deionized water with concentration of 1000 ppm. A blank sample containing deionized water without metal ions was used for blank.

The response variable was defined as the change in the SPR absorbance after exposure to metal ions. A metal interference was tested by measuring the absorbance portion of two metal ions between the metal selected. The interferent ions (all metal ions used except Hg2+) were evaluated at the same concentration as Hg2+ (1000 ppm), and the interference effect was assessed by comparing the analytical response obtained for Hg2+ in the absence and presence of the interferent. Linearity and sensitivity were carried out by dipping the chitosan-starch-Ag nanocomposite film with Hg2+ ions at concentration of 0, 2, 4, 6, 8, and 10 ppm to make curve calibration. Linear regression was performed using the calibration curve, and the coefficient of determination (R^2) was used to evaluate linearity, while slope (σ) was used to evaluate sensitivity. The SPR band within the 300–600 nm wavelength range was examined using a Shimadzu 1900i spectrophotometer. As for the LOD and LOQ they were calculated according to Eq. (1), where SD represents the standard deviation obtained with Standard Error of Estimate (residual standard deviation) method and slope obtained from calibration curve [18]. The resulting UV–Vis spectra were analyzed and visualized with OriginPro 2018 software.

$$\mathrm{LOD} = \frac{3\mathrm{xSD}}{\mathrm{Slope}} \quad \text{.....(1)}$$

$$\mathrm{LOQ} = \frac{10\mathrm{xSD}}{\mathrm{Slope}} \quad \text{.....(2)}$$

RESULTS AND DISCUSSION

1. Flavonoid Test of Tulsi Leaf Extract by Thin-layer Chromatography

Flavonoids are phytochemical compounds that can act as reducing agents. *Ocimum sanctum* is a natural source rich in polyphenolic and flavonoid compounds, including Vicenin 2, Luteolin-7-O-glucuronide, Isorientin, Orientin, Galuteolin, Apigenin-7-O-glucuronide, Vitexin, Isovitexin, Rosmarinic acid, Chlorogenic acid, Aesculin, Quercetin, Luteolin, Apigenin, and Caffeic acid [15], [18], [19]. These antioxidant compounds contain hydroxyl (–OH) groups that contribute to the reduction of Ag^+ to Ag^0[20]. TLC screening was performed to confirm flavonoid presence in the extract. As shown in Figure 1, the ethyl acetate fraction exhibited a yellow spot at an Rf value of 0.33 after spraying with 1% ethanolic aluminum chloride reagent, indicating flavonoid presence [17]. UV illumination at 254 nm also showed clear separation with distinct fractions.

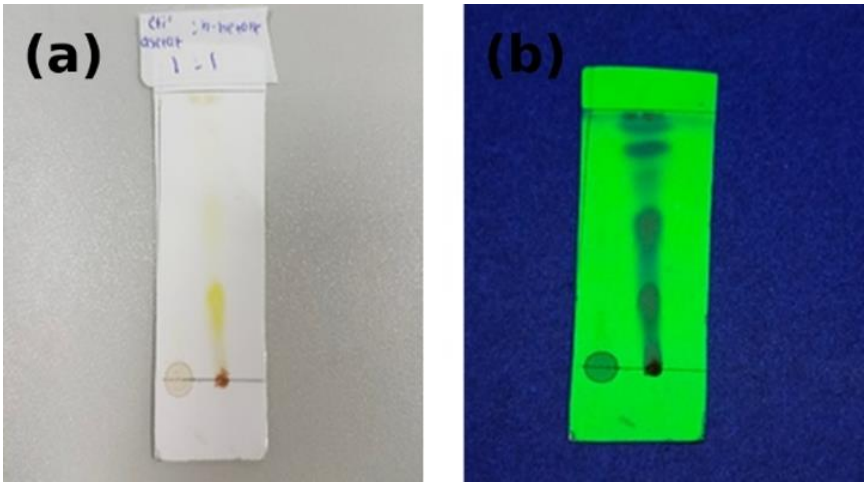

Figure 1. TLC screening results (a) after spraying with 1% AlCl3 reagent and (b) under UV light at 254 nm

2. Characterization of Tulsi Leaf Extract Using LC-MS

LC–MS analysis tentatively identified several metabolites belonging to the flavonoid, phenylpropanoid, and terpenoid classes, as presented in Table 1. Among these tentatively identified compounds, luteolin and apigenin exhibited the highest LC–MS signal intensities, with retention times of 7.73 min (m/z 287.0562) and 8.31 min (m/z 271.0623), respectively, as shown in the LC–MS chromatogram in Figure 2. These findings are consistent with those reported in [15], which identified luteolin and apigenin in Tulsi leaf extracts. Similarly, the presence of luteolin and apigenin has been reported in ethanolic and methanolic extracts of Tulsi leaves [18], [19]. The detection of these flavonoid compounds is relevant to AgNP synthesis because flavonoids contain hydroxyl groups that may participate in electron-donating reactions and interact with the nanoparticle surface during the reduction and stabilization processes [14]. However, the relatively high LC–MS signal intensities of luteolin and apigenin should not be interpreted as direct evidence of higher concentrations or as indicating a dominant contribution to Ag+ reduction, because LC–MS signal intensity is strongly influenced by ionization efficiency, which varies depending on the physicochemical properties of each compound and other instrumental factors. Therefore, the relative contribution of individual metabolites to the reduction process cannot be determined solely from LC–MS peak intensities. Nevertheless, the tentative identification of several flavonoid, phenylpropanoid, and terpenoid compounds indicates that Tulsi leaf extract contains a diverse range of phytochemicals that may collectively contribute to the formation and stabilization of AgNPs. In particular, luteolin and apigenin, as flavonoids containing multiple hydroxyl groups, may contribute to the reduction activity involved in AgNP synthesis [14].

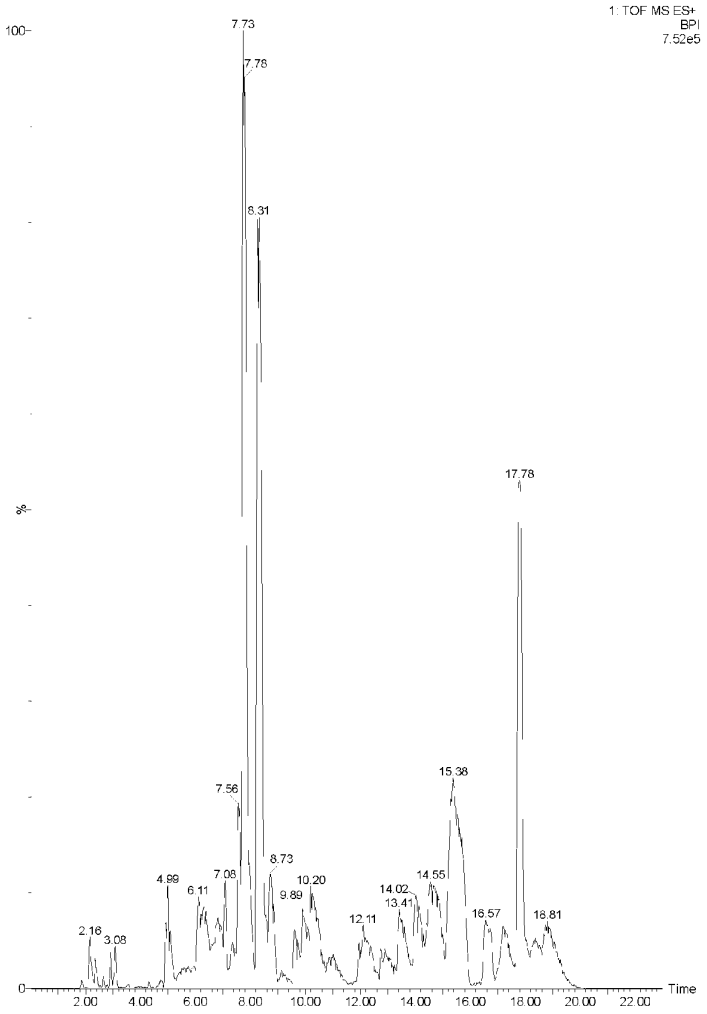

Figure 2. LC–MS chromatogram of Tulsi leaf extract

Table 1. LC-MS result of Tulsi leaf extract

RT	Positive Ion Mode m/z ([M+H]+)	Calculated m/z	Formula	Tentatively Annotated Compound	Group
5.100	209.1548	208.1546	$C_{13}H_{20}O_2$	Theaspirone	Terpenoid
6.245	299.1262	298.294	$C_{17}H_{14}O_5$	Apigenin 7,4′-dimethyl ether	Flavonoid
6.310	197.1192	196.1145	$C_{11}H_{16}O_3$	Loliolide	Terpenoid
6.510	179.1077	178 231	$C_{11}H_{14}O_2$	Methyl Eugenol	Phenylpropanoid
6.990	375.1462	374.345	$C_{19}H_{18}O_8$	Hymenoxin	Flavonoid
7.730	287.0565	286.0550	$C_{15}H_{10}O_6$	Luteolin	Flavonoid
8.312	271.0623	270.0600	$C_{15}H_{10}O_5$	Apigenin	Flavonoid
8.730	191.1448	190.1430	$C_{13}H_{18}O$	Damascenone	Terpenoid

3. Synthesis of Nanoparticles

Figure 3 shows a comparison of AgNPs synthesized using unfractionated and fractionated Tulsi leaf extracts. AgNPs synthesized using the unfractionated extract exhibited a more intense color compared to those synthesized using the fractionated extract, indicating a difference in their optical

response. The corresponding SPR spectra are presented in Figure 4. AgNPs synthesized using the unfractionated extract showed higher SPR intensity compared to those synthesized using the fractionated extract. However, SPR absorbance is influenced by several factors, including particle size, morphology, dispersion state, and the local dielectric environment. Therefore, the difference in SPR intensity reflects differences in the optical characteristics of the AgNPs dispersions and should not be directly interpreted as a quantitative measure of nanoparticle yield [21]. Furthermore, AgNPs synthesized using the fractionated extract exhibited a red-shift in the maximum SPR wavelength compared to those synthesized using the unfractionated extract. This shift may be attributed to differences in particle size and/or aggregation state, as an increase in particle size or aggregation can generally cause the SPR band to shift toward longer wavelengths [22]. Based on the preliminary evaluation of AgNPs synthesis using the unfractionated extract, a formulation consisting of 8% unfractionated Tulsi leaf extract and 3 mM $AgNO_3$ at pH 8 and 55°C, with a reaction time of 75 minutes, was selected for subsequent experiments. As for fractionated extract, a formulation consisting of 80 ppm unfractionated Tulsi leaf extract and 10 mM $AgNO_3$, with a reaction time of 120 minutes, was selected for subsequent experiments. These conditions were kept constant during the subsequent characterization and sensor development experiments.

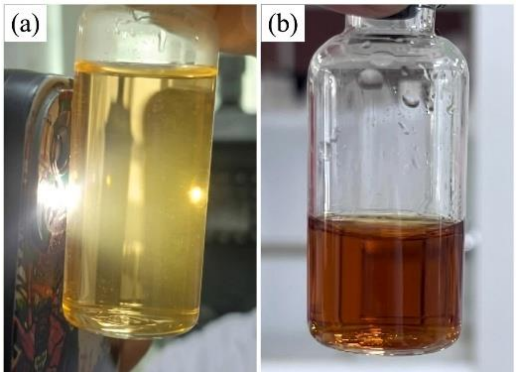

Figure 3. AgNPs synthesized using (a) unfractionated and (b) fractionated Tulsi leaf extracts

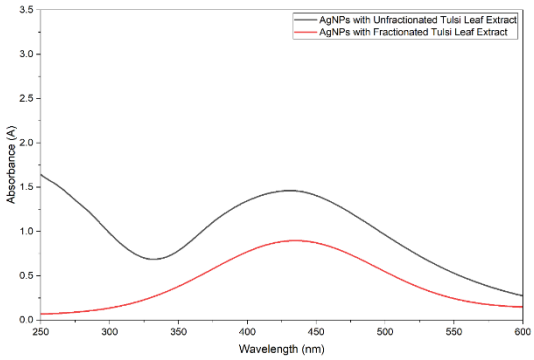

Figure 4. SPR spectra of AgNPs synthesized using unfractionated and fractionated extracts

4. Characterization of Silver Nanoparticles

Both types of AgNPs were subsequently characterized using PSA to determine particle size, polydispersity index (PDI), and zeta potential. Table 2 summarizes the PSA results for AgNPs synthesized using unfractionated (crude) and fractionated Tulsi leaf extracts. The results were obtained from three replicates and are presented as mean values ± standard deviation. AgNPs synthesized using the unfractionated extract exhibited a smaller average particle size (66.8 ± 1.0 nm) than those synthesized using the fractionated extract (185.7 ± 5.2 nm). The larger apparent

particle size of AgNPs derived from the fractionated extract may indicate a greater tendency toward aggregation or agglomeration, resulting in a larger hydrodynamic size [23]. Furthermore, AgNPs synthesized using the unfractionated extract showed a lower average PDI value (0.295 ± 0.024) than those synthesized using the fractionated extract (0.339 ± 0.031). The PDI reflects the breadth of the particle size distribution, with values approaching zero indicating a narrower distribution [24]. However, the PDI values obtained in this study indicate that both AgNP dispersions exhibited relatively broad particle size distributions rather than completely uniform particle populations.

The zeta potential of AgNPs synthesized using the unfractionated extract was −26.9 ± 1.0 mV, whereas AgNPs synthesized using the fractionated extract exhibited a value close to neutral (+0.5 ± 0.2 mV). Zeta potential provides an indication of the electrostatic contribution to colloidal stability. However, the commonly used ±30 mV criterion should be regarded as a general guideline rather than as absolute evidence of colloidal stability [25]. Thus, the higher absolute zeta potential value of AgNPs synthesized using the unfractionated extract indicates a greater electrostatic contribution to particle stabilization than that observed for AgNPs synthesized using the fractionated extract, although the value remains close to the frequently cited ±30 mV threshold. The observed differences between the two preparations may be associated with the removal of ethyl acetate-soluble phytochemicals during the fractionation process, which likely reduced the availability of compounds capable of acting as reducing, capping, or stabilizing agents. In addition, the use of methanol for redissolution may have altered the solvent environment and the interactions between phytochemicals and the AgNP surface [26]. Overall, under the investigated conditions, AgNPs synthesized using the unfractionated extract exhibited smaller particle sizes, lower PDI values, and higher absolute zeta potential values than those synthesized using the fractionated extract. Further characterization was performed on AgNPs synthesized using unfractionated Tulsi leaf extract. Figure 5 displays the FTIR spectra of the AgNPs and the Tulsi leaf extract. Both spectra exhibit broad bands at 3303 cm^{-1} for the AgNPs and 3307 cm^{-1} for the leaf extract, which can be attributed to O – H stretching vibrations from compounds containing hydroxyl groups. Weak bands were also observed near 2380 cm^{-1} (2382 cm^{-1} for AgNPs and 2381 cm^{-1} for the leaf extract). These bands are not associated with specific functional groups of the samples, as absorption in this region is generally related to atmospheric CO_2 and may arise from differences in atmospheric background during FTIR measurements. A band at 1636 cm^{-1} was observed in both spectra and may be associated with C=O or other oxygen-containing organic functional groups. The presence of these organic functional groups in both the leaf extract and the AgNPs indicates that plant-derived compounds remain associated with the AgNPs surface and likely contribute to the

capping and stabilization processes [27]. Similar FTIR-based interpretations have been reported for plant-synthesized AgNPs, where hydroxyl, carbonyl, and other organic functional groups are linked to phytochemicals involved in surface capping and stabilization [28]. However, FTIR analysis alone cannot confirm the reduction of Ag^{+} to Ag^{0} nor determine the specific contribution of each functional group to the reduction process

Table 2. Summary of results from PSA

	Replications	AgNPs with Unfractionated Extract	AgNPs with Fractionated Extract
Particle Size (nm)	1	68.0	185.3
	2	66.2	180.7
	3	66.3	191.1
Average (nm)		66.8	185.7
Polydispersity Index	1	0.273	0.336
	2	0.321	0.371
	3	0.292	0.310
Average		0.295	0.339
Zeta Potential (mV)	1	-26.5	+0.3
	2	-26.3	+0.7
	3	-28.1	+0.5
Average (mV)		-26.9	+0.5

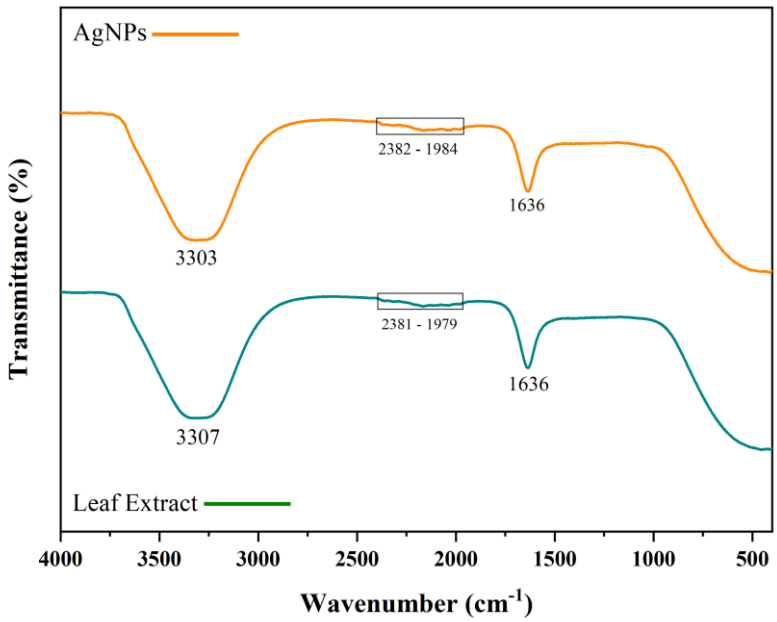

Figure 5. FTIR spectra of AgNPs and tulsi leaf extract

5. Characterization of Chitosan-starch-Ag Nanocomposite Film

AgNPs synthesized with extract without fractionation were then modified into nanocomposites using chitosan-starch to obtain a chitosan-starch-Ag nanocomposite film which is then called AgNCF. The combination of starch and chitosan in this

system occurs through physical interactions in the form of hydrogen bonds between the functional groups present in the two biopolymers. When starch and chitosan are mixed in solution, the –OH groups of starch can interact with the –OH and –NH2 groups of chitosan through hydrogen bonding. This interaction results in the formation of a stable mixed polymer network without the formation of new covalent bonds[29]. Figure 6(a) is the SPR spectra for chitosan-starch, AgNCF, and AgNPs. In the AgNCF spectrum, the SPR peak of silver nanoparticles is still observed around 433 nm, but with a lower absorbance intensity compared to AgNPs in solution form. This decrease in intensity was caused by the encapsulation and immobilization of AgNPs in the starch chitosan matrix, which limits the mobility of surface electrons and increases light scattering by the polymer matrix [30].

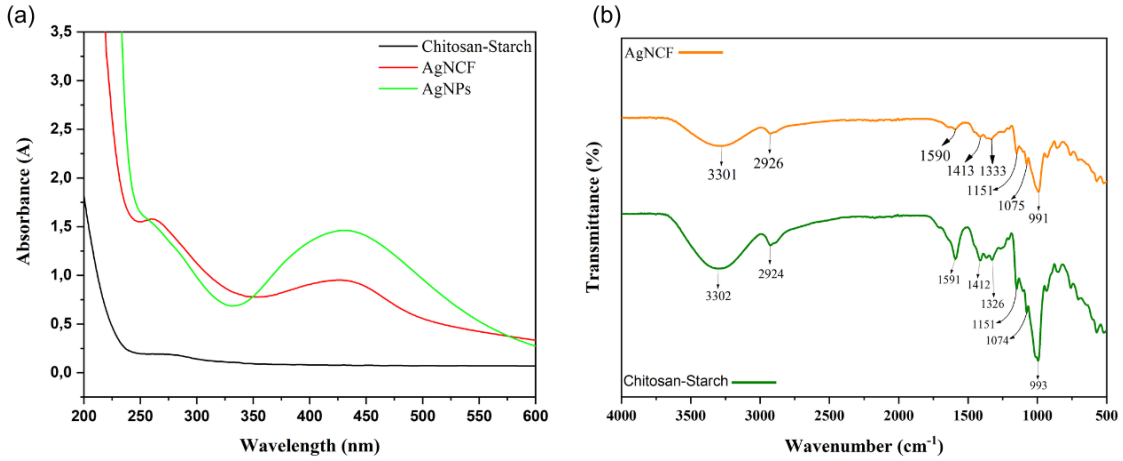

Figure 1. (a) SPR spectra of chitosan–starch, AgNCF, and AgNPs, (b) FTIR spectra of chitosan–starch and AgNCF

The FTIR spectrum Figure 6(b) shows a broad absorption band at a wave number of around 3302 cm-1, which indicates the presence of O–H and N–H groups derived from starch and chitosan. The absorption band at 2924 cm-1 is related to the C–H stretching vibration in the starch structure. The interaction between the hydroxyl groups of starch and the amino groups in chitosan is indicated by the presence of an absorption band at 1591 cm-1. Furthermore, the band at 1151 cm-1 represents the stretching vibration of the C–O bond. Symmetric vibration –CH was observed at wave number 1412 cm-1, while the peak at 1,074 cm-1 indicated the presence of C–O/C–O–C stretching vibrations typical of starch and chitosan polysaccharide structures, while the peak at 1074 cm-1 indicated the presence of C–O/C–O–C bond vibrations Comparison of the FTIR spectra between the chitosan-starch matrix and the AgNCF reveals no significant shifts in functional groups or noticeable changes in intensity within the limits of the observational resolution. This spectral similarity indicates that the addition of silver nanoparticles does not substantially alter the primary covalent bonds within the polymer matrix, or that the interaction between the nanoparticles and the matrix is predominantly physical in nature and falls below the sensitivity threshold of the FTIR analysis under the tested conditions [30].

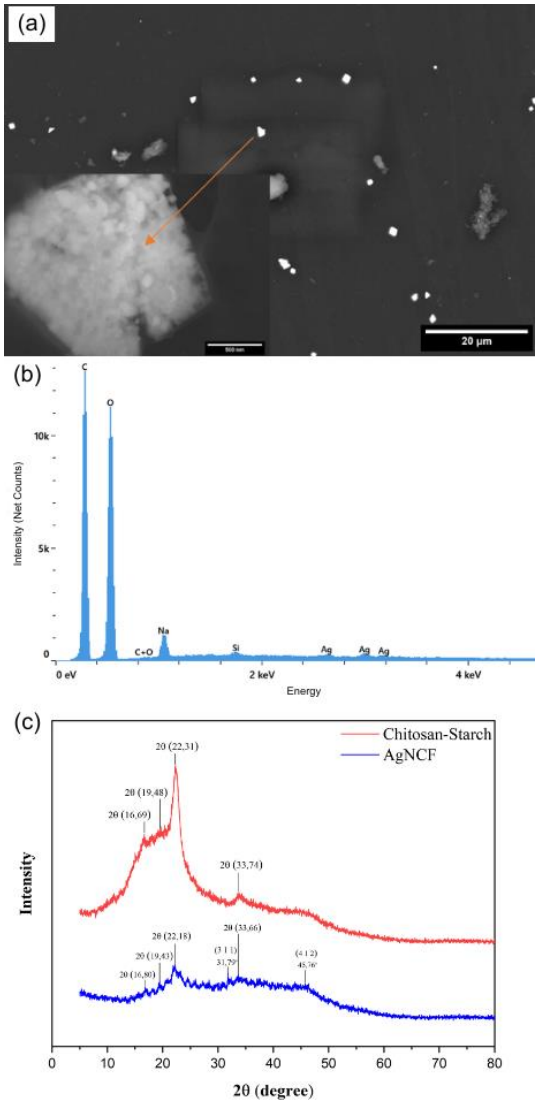

Figure 2. (a) SEM image of AgNCF (1,200× magnification, accelerating voltage of 20 kV, working distance of 9.09 mm, and scale bar of 20 µM & 500 nm), (b) EDX spectrum of AgNCF, and (c) XRD patterns of AgNCF and chitosan–starch

SEM and EDX analyses were conducted to characterize the surface morphology and elemental composition of AgNCF. The SEM image (Figure 7 (a)) reveals an irregular and heterogeneous surface morphology, with bright particle-like features and relatively large clustered regions, as indicated by the arrows. These features may represent Ag-containing particles or agglomerates [31]. However, SEM morphology alone cannot definitively distinguish individual AgNPs from agglomerates or from features originating from the underlying polymer matrix. The EDX spectrum (Figure 7(b)) shows prominent C and O signals consistent with the starch–chitosan matrix, together with a characteristic Ag signal at approximately 3 keV, confirming the presence of Ag in the analyzed region [32]. Quantitative EDX analysis across seven areas showed Ag contents ranging from 0.0 to 28.9 wt%, while the C and O contents ranged from 25.2–40.0 wt% and 44.5–61.0 wt%, respectively. The substantial variation in Ag content among the analyzed areas indicates a heterogeneous surface distribution of Ag. Therefore, although the EDX results confirm the presence of Ag in the film, they should not be interpreted as direct evidence of a uniform nanoscale dispersion of AgNPs throughout the polymer matrix.

The XRD pattern of the chitosan–starch film (Figure 7(c)) exhibits broad diffraction features at 2θ ≈ 16.69°, 19.48°, and 22.31°, indicating a predominantly semicrystalline structure with a substantial amorphous contribution. These diffraction features are consistent with the crystalline contributions of the starch–chitosan matrix, as starch typically exhibits reflections within the 15–23° range, whereas chitosan-based films show broad diffraction features around 19–22° [33]. Following the incorporation of AgNPs, the main diffraction features of the chitosan–starch matrix remained at approximately 16.80°, 19.43°, and 22.18°, suggesting that

the overall structural characteristics of the polymer matrix were preserved. Additional reflections were observed at approximately 31.79° and 45.76°. However, these peaks cannot be conclusively assigned to metallic Ag based solely on their positions. Face-centered cubic metallic Ag is typically characterized by reflections near 38°, 44°, 64°, and 77°, corresponding to the (111), (200), (220), and (311) planes, respectively [34]. Therefore, the additional peaks at 31.79° and 45.76° are more appropriately reported as unidentified reflections pending comparison with suitable reference diffraction patterns.

6. Sensor Performance Tests

Figure 8 shows the color changes observed for AgNPs synthesized using the unfractionated extract, both in colloidal and film forms. A distinct color change in response to Hg^{2+} was observed only for AgNCF. Changes in the SPR intensity of AgNCF during the selectivity and interference tests are shown in Figure 9(a) and Figure 9(b). The largest change in SPR intensity was observed in the presence of Hg^{2+}, while the presence of other metal ions did not significantly interfere with the AgNCF signal response. The high selectivity of AgNCF toward Hg^{2+} may be associated with a redox reaction and the formation of an Ag–Hg amalgam, in which Hg^{2+} is reduced to Hg^{0} and subsequently interacts with Ag on the nanoparticle surface. This process decreases the intensity of the SPR peak, resulting in a large change in absorbance (Δ absorbance). In contrast, the other metal ions do not exhibit sufficient affinity toward AgNCF to induce significant optical changes [35].

Figure 9(c) illustrates the SPR spectra of AgNCF recorded weekly over four weeks of storage at room temperature (~25°C) under indoor relative humidity conditions. The SPR band of the AgNPs remained detectable within the 400–420 nm range throughout the four-week storage period, while the characteristic visual color was retained without noticeable macroscopic fading. A slight red shift in the peak wavelength was observed over time, accompanied by an increase in absorbance intensity. Although the persistence of the SPR peak indicates the relative optical stability of the AgNPs within the starch–chitosan matrix, the slight spectral shift and baseline drift may reflect minor structural rearrangements, solvent evaporation, or subtle changes in nanoparticle dispersion during storage rather than an improvement in stability [36], [37]. The sensor response-time test showed that the response time increased as the Hg^{2+} concentration decreased. At 100 ppm, the color change became visible after 23 s and reached a stable response after 3 min 2 s, whereas at 5 ppm, the color change became visible after 62 s and stabilized after 7 min 14 s. These results indicate that higher Hg^{2+} concentrations accelerate the Ag–Hg interaction, resulting in a faster sensor response and a shorter time required to reach a stable signal.

Figure 9(d) shows the calibration curve of the AgNCF sensor for Hg^{2+} detection based on absorbance values measured at 433 nm. The absorbance decreased linearly with increasing Hg^{2+} concentration within the investigated range of 0–10 ppm, following the regression equation $y = -0.04813x + 0.66931$ with $R^2 = 0.99757$. This R^2 value indicates a

strong linear relationship between Hg^{2+} concentration and the sensor response [38]. The decrease in absorbance is likely attributable to the interaction between Hg^{2+} and AgNPs, which alters the surface plasmon resonance (SPR) response of the nanocomposite film [30]. The absolute value of the calibration-curve slope (0.04813 absorbance units ppm^{-1}) represents the analytical sensitivity of the sensor within the investigated concentration range. The residual standard deviation obtained from the calibration regression was 0.00995, and this value was used to estimate the LOD and LOQ. Based on the equations described in the analytical method, the LOD and LOQ were calculated to be 0.68 ppm and 2.07 ppm, respectively. Therefore, although the calibration curve was constructed using Hg^{2+} concentrations of 0, 2, 4, 6, 8, and 10 ppm, the quantitative range should be interpreted in relation to the calculated LOQ rather than being reported as a fully validated quantitative range beginning at 0 ppm.

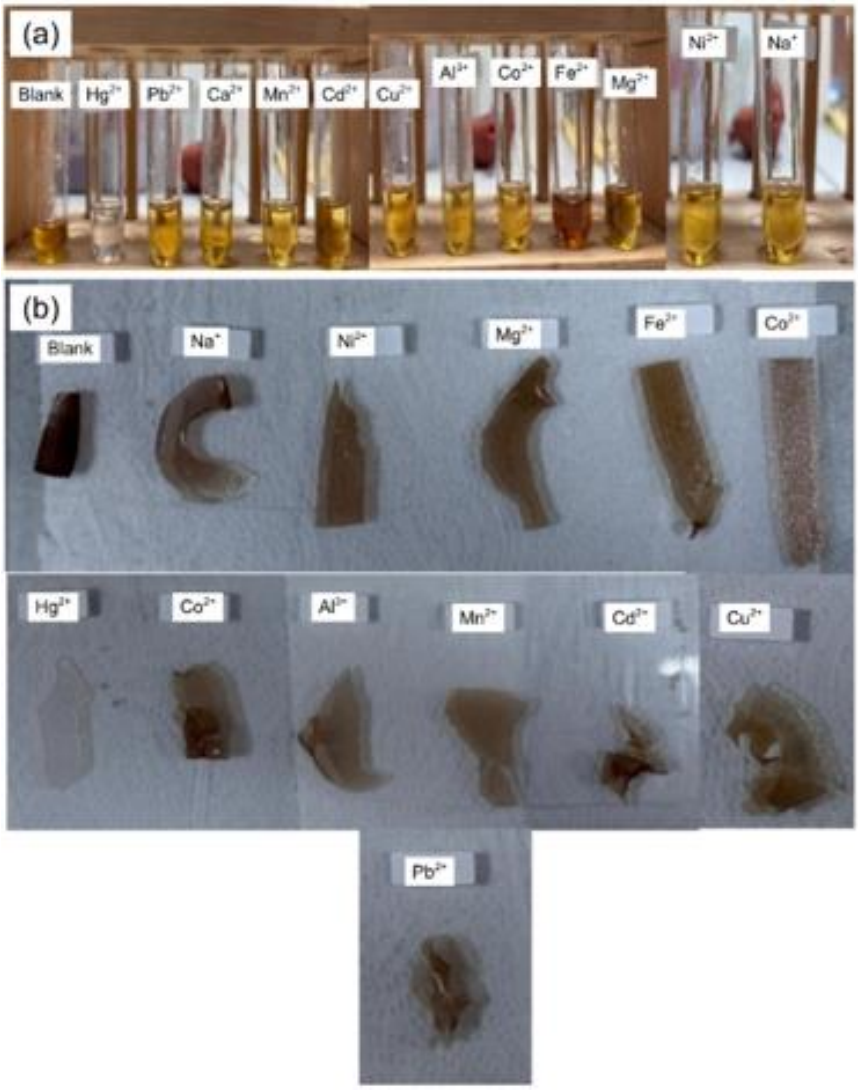

Figure 3. Visual selectivity test of (a) AgNPs, (b) AgNCF toward the tested metal ions

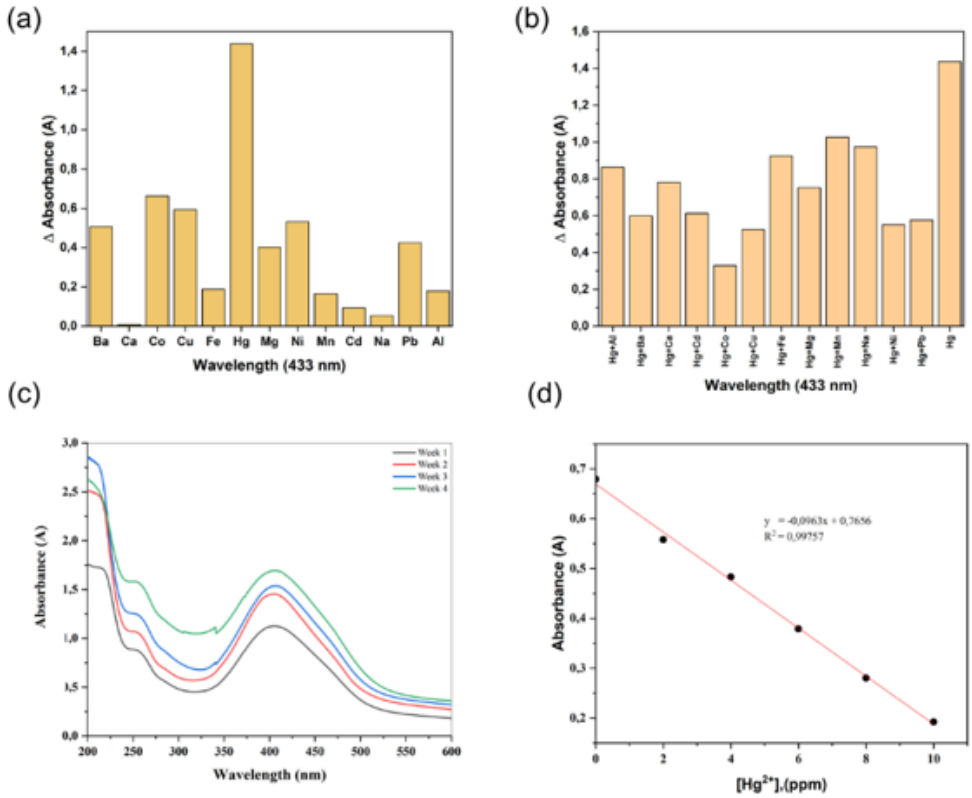

Figure 4. (a) Selectivity response of AgNCF at 433 nm, (b) Interference response of AgNCF in the presence of competing metal ions, (c) SPR spectra of AgNCF during four weeks of storage, (d) Calibration curve for Hg^{2+} determination using AgNCF

CONCLUSION

AgNPs were successfully synthesized using unfractionated and fractionated Tulsi leaf extract. AgNPs synthesized using unfractionated Tulsi leaf extract had better characteristics (higher SPR intensity, smaller size, and better stability), where AgNPs were synthesized at a reaction time of 75 minutes, 3 mM $AgNO_3$, 8% v/v extract, and pH 8. The resulting AgNPs had an SPR peak of around 430 nm, an average size of 66.8 nm, a PDI of 0.295, and a zeta potential of −26.9 mV indicating good stability. AgNCF based on starch-chitosan-AgNPs was also successfully synthesized with the formation of a silver crystalline phase and a characteristic color change. AgNCF showed good performance as a selective Hg^{2+} sensor with linear working range of 0 – 10 ppm Hg^{2+} (R^2 = 0.99757), and LOD of 0.68 ppm and LOQ of 2.07 ppm. This sensor has the potential to be used as a colorimetric sensor for detecting Hg^{2+}, however, performance improvements are required to achieve a low LOD that meets regulatory standards.

Author Contributions: Y. Pratiwi contributed to the conceptualization, methodology, experimental design, and manuscript preparation; F. A. Asyifa contributed to laboratory experiments and data collection; A. Darmawan contributed to characterization analysis and data interpretation; H. A. Khansa served as the corresponding author and contributed to

supervision, validation, and manuscript revision; E. V. Nanda contributed to data analysis and visualization; B. A. Riyandari contributed to literature review and scientific discussion; A. S. M. Ajeetha contributed to manuscript review and editing. All authors reviewed and approved the final version of the manuscript.

Conflict of Interest: The authors declare that they have no known competing financial interests or personal relationships that could have influenced the work reported in this manuscript.

Declaration of Generative AI and AI-Assisted Technologies: Generative artificial intelligence (AI) tools were used during the preparation of this manuscript solely to assist in the development of the graphical abstract and to improve the English language through proofreading and grammatical correction. The authors reviewed and edited all AI-assisted outputs and take full responsibility for the final content of the manuscript.

REFERENCES

[1] F. A. Idrus and V. U. Ding, "Heavy metal contamination in sediments of the Sematan-Serayan River, Sarawak: Assessment of pollution indices and environmental risk implications," Environ. Monit. Assess., vol. 198, no. 3, Art. no. 253, Feb. 2026, doi: https://doi.org/10.1007/s10661-026-15110-w.

[2] K. F. Kayani and S. J. Mohammed, "Mercury in aquatic environments: toxicity and advances in remediation using covalent organic frameworks," Mater. Adv., vol. 6, no. 11, pp. 3371–3385, 2025, doi: https://doi.org/10.1039/D5MA00208G.

[3] Kementerian Lingkungan Hidup dan Kehutanan, "Peraturan Pemerintah Republik Indonesia No. 22 Tahun 2021 tentang Penyelenggaraan Perlindungan dan Pengelolaan Lingkungan Hidup," Sekretariat Negara, Jakarta, Indonesia, 2021.

[4] E. K. Sembiring, L. Fitria, H. Kusnoputranto, and A. J. Kario, "Evaluation of Mercury (Hg) Concentration in Cilemahabang River, Bekasi Regency," PREPOTIF: Jurnal Kesehatan Masyarakat, vol. 9, no. 1, pp. 969–973, Apr. 2025, doi: https://doi.org/10.31004/prepotif.v9i1.43419.

[5] A. Asaduzzaman et al., "Environmental Mercury Chemistry – In Silico," Acc. Chem. Res., vol. 52, no. 2, pp. 379–388, Feb. 2019, doi: https://doi.org/10.1021/acs.accounts.8b00454.

[6] B. Liu, J. Zhuang, and G. Wei, "Recent advances in the design of colorimetric sensors for environmental monitoring," Environ. Sci. Nano, vol. 7, no. 8, pp. 2195–2213, 2020, doi: https://doi.org/10.1039/D0EN00449A.

[7] A. Khatoon, J. A. Syed, A. R. Solangi, A. Mallah, and Sirajuddin, "Mechanistic insights of mercury ion detection and its influence on time monitored hydrodynamic size of Capsicum Annumm C derived silver nanoparticles during colorimetric nano-sensing," Optik, vol. 325, Art. no. 172237, Apr. 2025, doi: https://doi.org/10.1016/j.ijleo.2025.172237.

[8] Y. Pratiwi, Y. Febrian, L. E. Anggraini, H. A. Khansa, and R. C. Widianti, "Green Synthesis of Silver Nanoparticles using Lemongrass Leaf (Cymbopogon citratus) Extract as a Reductant for Novel Colorimetric Mercury(II) Detection," JKPK (Jurnal Kimia dan Pendidikan Kimia), vol. 10, no. 3, 2025, doi: https://doi.org/10.20961/jkpk.v10i3.109804.

[9] G. M. Sangaonkar, M. P. Desai, T. D. Dongale, and K. D. Pawar, "Selective

interaction between phytomediated anionic silver nanoparticles and mercury leading to amalgam formation enables highly sensitive, colorimetric and memristor-based detection of mercury," Sci. Rep., vol. 10, no. 1, Art. no. 2037, Feb. 2020, doi: https://doi.org/10.1038/s41598-020-58844-4.

[10] Z. Zulfiqar et al., "Plant-mediated green synthesis of silver nanoparticles: Synthesis, characterization, biological applications, and toxicological considerations: A review," Biocatal. Agric. Biotechnol., vol. 57, Art. no. 103121, Apr. 2024, doi: https://doi.org/10.1016/j.bcab.2024.103121.

[11] S. Thomas, R. A. Gonsalves, J. Jose, S. H. Zyoud, A. R. Prasad, and J. Garvasis, "Plant-based synthesis, characterization approaches, applications and toxicity of silver nanoparticles: A comprehensive review," J. Biotechnol., vol. 394, pp. 135–149, Nov. 2024, doi: https://doi.org/10.1016/j.jbiotec.2024.08.009.

[12] A. Dhaka, S. Chand Mali, S. Sharma, and R. Trivedi, "A review on biological synthesis of silver nanoparticles and their potential applications," Results Chem., vol. 6, Art. no. 101108, Dec. 2023, doi: https://doi.org/10.1016/j.rechem.2023.101108.

[13] C. Pattnaik et al., "Green synthesis of glucose-capped stable silver nanoparticles: a cost-effective sensor for the selective detection of Hg2+ ions in aqueous solutions," Sensors Diagn., vol. 2, no. 3, pp. 647–656, 2023, doi: https://doi.org/10.1039/D3SD00019B.

[14] N. A. N. Mohamad, N. A. Arham, J. Jai, and A. Hadi, "Plant Extract as Reducing Agent in Synthesis of Metallic Nanoparticles: A Review," Adv. Mater. Res., vol. 832, pp. 350–355, Nov. 2013, doi: https://doi.org/10.4028/www.scientific.net/AMR.832.350.

[15] A. Chaudhary, S. Sharma, A. Mittal, S. Gupta, and A. Dua, "Phytochemical and antioxidant profiling of Ocimum sanctum," J. Food Sci. Technol., vol. 57, no. 10, pp. 3852–3863, Oct. 2020, doi: https://doi.org/10.1007/s13197-020-04417-2.

[16] F. Eker, E. Akdaşçi, H. Duman, M. Bechelany, and S. Karav, "Green Synthesis of Silver Nanoparticles Using Plant Extracts: A Comprehensive Review of Physicochemical Properties and Multifunctional Applications," Int. J. Mol. Sci., vol. 26, no. 13, Art. no. 6222, Jun. 2025, doi: https://doi.org/10.3390/ijms26136222.

[17] L. Gwatidzo, P. Dzomba, and M. Mangena, "TLC separation and antioxidant activity of flavonoids from Carissa bispinosa, Ficus sycomorus, and Grewia bicolar fruits," Nutrire, vol. 43, no. 1, Art. no. 3, Dec. 2018, doi: https://doi.org/10.1186/s41110-018-0062-5.

[18] M. P. Venuprasad, H. K. Kandikattu, S. Razack, N. Amruta, and F. Khanum, "Chemical composition of Ocimum sanctum by LC-ESI–MS/MS analysis and its protective effects against smoke induced lung and neuronal tissue damage in rats," Biomed. Pharmacother., vol. 91, pp. 1–12, Jul. 2017, doi: https://doi.org/10.1016/j.biopha.2017.04.011.

[19] R. Pandey, P. Chandra, M. Srivastava, D. K. Mishra, and B. Kumar, "Simultaneous quantitative determination of multiple bioactive markers in Ocimum sanctum obtained from different locations and its marketed herbal formulations using UPLC-ESI-MS/MS combined with principal component analysis," Phytochem. Anal., vol. 26, no. 6, pp. 383–394, Nov. 2015, doi: https://doi.org/10.1002/pca.2551.

[20] M. Ismail et al., "Phytosynthesis of silver nanoparticles; naked eye cellulose filter paper dual mechanism sensor for mercury ions and ammonia in aqueous solution," J. Mater. Sci.: Mater. Electron., vol. 30, no. 8, pp. 7367–7383, Apr. 2019, doi: https://doi.org/10.1007/s10854-019-01049-x.

[21] Q.-A. Trieu, Q. N. Ai Ung, P. N. Thai, T. M. Mai, and D. Van Nguyen, "Harnessing nature for dual action: silver

nanoparticles synthesized from guava leaf extract for photocatalytic degradation of methyl red and antibacterial applications," RSC Adv., vol. 15, no. 17, pp. 13353–13363, 2025, doi: https://doi.org/10.1039/D5RA02503F.

[22] Y. Li, Q. Liao, W. Hou, and L. Qin, "Silver-Based Surface Plasmon Sensors: Fabrication and Applications," Int. J. Mol. Sci., vol. 24, no. 4, Art. no. 4142, Feb. 2023, doi: https://doi.org/10.3390/ijms24044142.

[23] J.-M. Teulon et al., "On the Operational Aspects of Measuring Nanoparticle Sizes," Nanomaterials, vol. 9, no. 1, Art. no. 18, Dec. 2018, doi: https://doi.org/10.3390/nano9010018.

[24] I. I. Latumakulita and S. Suparno, "Characterization of Silver Nanoparticle Electrolysis Method with UV-Vis Spectrometer, Atomic Absorption Spectrophotometer, and Particle Size Analyzer," Kasuari: Phys. Educ. J., vol. 5, no. 1, pp. 42–52, Jun. 2022, doi: https://doi.org/10.37891/kpej.v5i1.178.

[25] D. J. Pochapski, C. Carvalho dos Santos, G. W. Leite, S. H. Pulcinelli, and C. V. Santilli, "Zeta Potential and Colloidal Stability Predictions for Inorganic Nanoparticle Dispersions: Effects of Experimental Conditions and Electrokinetic Models on the Interpretation of Results," Langmuir, vol. 37, no. 45, pp. 13379–13389, Nov. 2021, doi: https://doi.org/10.1021/acs.langmuir.1c02056.

[26] M. Khan et al., "Solvent based fractional biosynthesis, phytochemical analysis, and biological activity of silver nanoparticles obtained from the extract of Salvia moorcroftiana," PLoS One, vol. 18, no. 10, Art. no. e0287080, Oct. 2023, doi: https://doi.org/10.1371/journal.pone.0287080.

[27] S. Jain and M. S. Mehata, "Medicinal Plant Leaf Extract and Pure Flavonoid Mediated Green Synthesis of Silver Nanoparticles and their Enhanced Antibacterial Property," Sci. Rep., vol. 7, no. 1, Art. no. 15867, Nov. 2017, doi: https://doi.org/10.1038/s41598-017-15724-8.

[28] N. Liaqat, N. Jahan, Khalil-ur-Rahman, T. Anwar, and H. Qureshi, "Green synthesized silver nanoparticles: Optimization, characterization, antimicrobial activity, and cytotoxicity study by hemolysis assay," Front. Chem., vol. 10, Art. no. 952006, Aug. 2022, doi: https://doi.org/10.3389/fchem.2022.952006.

[29] L. Biao et al., "Synthesis, characterization and antibacterial study on the chitosan-functionalized Ag nanoparticles," Mater. Sci. Eng. C, vol. 76, pp. 73–80, Jul. 2017, doi: https://doi.org/10.1016/j.msec.2017.02.154.

[30] P. Dhanyasree, K. V. Neenu, D. Anna David, P. M. Sabura Begum, and K. Yoosaf, "An eco-friendly Polymer-Silver nanocomposite film for simultaneous sensing and removal of mercury from water," Microchem. J., vol. 207, Art. no. 112188, Dec. 2024, doi: https://doi.org/10.1016/j.microc.2024.112188.

[31] M. A. Ashraf, W. Peng, Y. Zare, and K. Y. Rhee, "Effects of Size and Aggregation/Agglomeration of Nanoparticles on the Interfacial/Interphase Properties and Tensile Strength of Polymer Nanocomposites," Nanoscale Res. Lett., vol. 13, no. 1, Art. no. 214, Dec. 2018, doi: https://doi.org/10.1186/s11671-018-2624-0.

[32] D. Martínez-Cisterna et al., "Chitosan-Coated Silver Nanocomposites: Biosynthesis, Mechanical Properties, and Ag+ Release in Liquid and Biofilm Forms," Int. J. Mol. Sci., vol. 26, no. 9, Art. no. 4130, Apr. 2025, doi: https://doi.org/10.3390/ijms26094130.

[33] L. Gao, T. Zhu, F. He, Z. Ou, J. Xu, and L. Ren, "Preparation and Characterization of Functional Films Based on Chitosan and Corn Starch Incorporated Tea Polyphenols," Coatings, vol. 11, no. 7, Art. no. 817, Jul. 2021, doi: https://doi.org/10.3390/coatings11070817.

[34] A. Hosney et al., “Green Synthesis of Chitosan Silver Nanoparticle Composite Materials: A Comparative Study of Microwave and One-Pot Reduction Methods,” Polymers, vol. 17, no. 21, Art. no. 2960, Nov. 2025, doi: https://doi.org/10.3390/polym17212960.

[35] P. O. Oladoye, G. Liu, Q. Zhang, and Y. Cai, “Reduction and amalgamation of mercury in silver nanoparticle suspensions under dark conditions,” Chemosphere, vol. 371, Art. no. 144035, Feb. 2025, doi: https://doi.org/10.1016/j.chemosphere.2024.144035.

[36] F. Y. Alzoubi, A. A. Ahmad, I. A. Aljarrah, A. B. Migdadi, and Q. M. Al-Bataineh, “Localize surface plasmon resonance of silver nanoparticles using Mie theory,” J. Mater. Sci.: Mater. Electron., vol. 34, no. 32, Art. no. 2128, Nov. 2023, doi: https://doi.org/10.1007/s10854-023-11304-x.

[37] H. Xue, L. Ji, K. Zhang, P. Wang, X. Liao, and J. Tan, “Preparation, properties, and applications of polysaccharide-based films: A comprehensive overview,” J. Future Foods, Aug. 2025, doi: https://doi.org/10.1016/j.jfutfo.2025.05.011.

[38] S. M. Moosavi and S. Ghassabian, “Linearity of Calibration Curves for Analytical Methods: A Review of Criteria for Assessment of Method Reliability,” in Calibration and Validation of Analytical Methods - A Sampling of Current Approaches, IntechOpen, 2018, doi: https://doi.org/10.5772/intechopen.72932.